

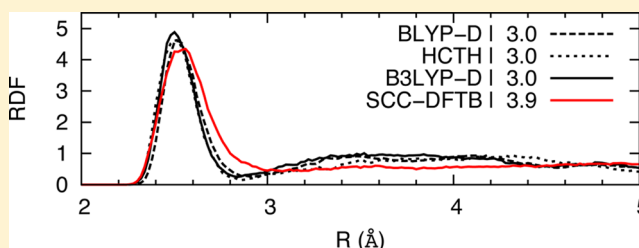
# Benchmark Study of the SCC-DFTB Approach for a Biomolecular Proton Channel

Ruibin Liang, Jessica M. J. Swanson, and Gregory A. Voth\*

Department of Chemistry, Institute for Biophysical Dynamics, James Franck Institute, and Computation Institute, University of Chicago, 5735 South Ellis Avenue, Chicago, Illinois 60637, United States of America

## Supporting Information

**ABSTRACT:** The self-consistent charge density functional tight binding (SCC-DFTB) method has been increasingly applied to study proton transport (PT) in biological environments. However, recent studies revealing some significant limitations of SCC-DFTB for proton and hydroxide solvation and transport in bulk aqueous systems call into question its accuracy for simulating PT in biological systems. The current work benchmarks the SCC-DFTB/MM method against more accurate DFT/MM by simulating PT in a synthetic leucine–serine channel (LS2), which emulates the structure and function of biomolecular proton channels. It is observed that SCC-DFTB/MM produces overcoordinated and less structured pore water, an overcoordinated excess proton, weak hydrogen bonds around the excess proton charge defect, and qualitatively different PT dynamics. Similar issues are demonstrated for PT in a carbon nanotube, indicating that the inaccuracies found for SCC-DFTB are not due to the point charge based QM/MM electrostatic coupling scheme, but rather to the approximations of the semiempirical method itself. The results presented in this work highlight the limitations of the present form of the SCC-DFTB/MM approach for simulating PT processes in biological protein or channel-like environments, while providing benchmark results that may lead to an improvement of the underlying method.



## INTRODUCTION

Calculations using *ab initio* quantum mechanical (QM) methods can in principle be quite accurate for describing various kinds of systems at the atomic level. QM methods are also well suited for describing chemical reactions in which bond breaking and formation occur. However, the cost of the QM calculations limits not only the system size but also the sampling that is required to calculate statistically meaningful quantities for condensed phase systems, such as free energies of binding or a potential of mean force (PMF) for solute or ion transport. Therefore, it is sometimes necessary to develop approximations to *ab initio* QM methods that offer a balance between accuracy and computational efficiency. The self-consistent charge density functional tight binding (SCC-DFTB) method<sup>1</sup> is a fast semiempirical QM algorithm that has become popular in recent years for simulating chemical processes in biomolecular systems due to the high degree of interest in studying such systems.<sup>2</sup> The SCC-DFTB method is derived from density functional theory (DFT) by approximation and parametrization of multicenter electron integrals.<sup>1</sup> The computational speed gained by these approximations can be 2–3 orders of magnitude compared to more accurate and “first principles” standard DFT.<sup>3</sup> While the SCC-DFTB approach is understandably popular, the method has been shown to have substantial limitations for predicting structural, energetic, and dynamic properties of proton transport (PT)<sup>4</sup> and hydroxide transport in bulk water.<sup>5</sup> Despite recent SCC-

DFTB developments,<sup>3,6,7</sup> these issues remain unresolved. The SCC-DFTB method was also, for example, recently shown to poorly describe noncovalent interactions involving sulfur atoms.<sup>8</sup> Given the increased use of quantum mechanics/molecular mechanics (QM/MM) with SCC-DFTB as the QM method (SCC-DFTB/MM) to study proton hydration and transport in biomolecular systems,<sup>9–11</sup> there is a need to benchmark its present level of accuracy and potential limitations in such environments.

The current work establishes a systematic benchmark of SCC-DFTB/MM method against arguably more accurate QM/MM methods that employ both generalized gradient approximation (GGA) level and hybrid-GGA level DFT theories for the QM calculation. The comparison is made in the context of condensed phase molecular dynamics (MD) simulations of PT in channel systems. All the methods under investigation have a comparable amount of sampling time, which has seldom been done to date. The synthetic leucine–serine channel (LS2, Figure 1)<sup>12</sup> is chosen as the simulation system. Although it is synthetic, LS2 possesses key features that are representative of proton channels in nature, such as high proton selectivity, a nonuniform pore radius along the channel axis, a hydrophilic pore due to pore-lining serine residues, and a macrodipole formed by parallelhelices.<sup>12–15</sup> In addition, it is

Received: September 22, 2013

Published: December 16, 2013

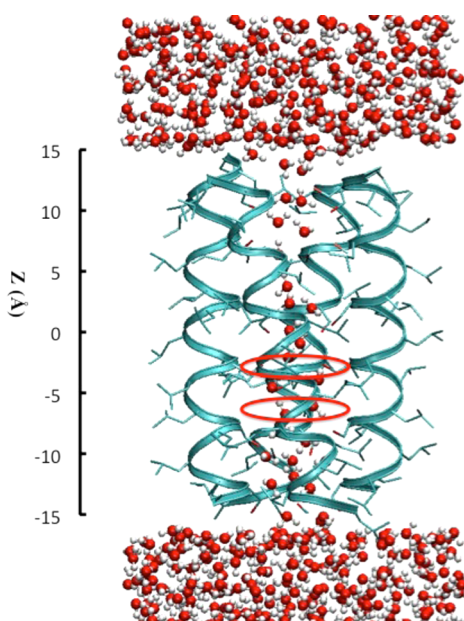


**Figure 1.** LS2 channel system filled with a protonated water wire. The two red circles denote the regions where the excess proton CEC is restrained in the QM/MM simulations. The protein backbones and side chains are depicted as the ribbons and sticks, respectively. On the left is the scale of the channel along the  $z$  direction.

small enough to enable sufficient sampling for the convergence of statistical quantities extracted from MD simulations, which is both essential for condensed phase analysis and computationally demanding for the higher level QM/MM approaches.

It has been argued<sup>6</sup> that the conclusions drawn from previous SCC-DFTB benchmark studies of PT in bulk water<sup>4</sup> may not be relevant to PT in the biological systems for two reasons: first, the charge delocalization of the excess protonic defect may be smaller in biological systems; and second, the  $pK_a$  values of biological titratable groups may dominate PT energetics. However, in this work, it is observed that the present ‘state-of-the-art’ SCC-DFTB method fails to reproduce important aspects of the more accurate DFT results in a channel environment. Furthermore, by also running simulations in a hydrophobic channel (a nanotube), it is shown that the inaccuracies of SCC-DFTB/MM are more related to the approximations of the semiempirical QM method itself, rather than to the approximations introduced by a simple point charge based QM/MM electrostatic coupling scheme.<sup>16</sup> These combined results provide an important benchmark of the current SCC-DFTB/MM method that can help researchers to gauge the reliability of this approach for studying PT in realistic biomolecular systems. These results can also help underpin possible improvement of the method if in fact such an improvement is possible without resorting to an excessive degree of empiricism that would undermine the purpose of a QM approach in the first place.

## METHODOLOGY

**2.1. SCC-DFTB Method.** The SCC-DFTB method is derived by Taylor series expansion of the DFT Kohn–Sham energy in terms of the charge density fluctuations, and the Hamiltonian matrix elements are evaluated using a minimal basis set of pseudoatomic orbitals with a two-center

approximation. The total energy for the full third order SCC-DFTB method is expressed as<sup>3</sup>

$$E_{\text{total}}^{\text{SCC-DFTB}} = \sum_{i\mu\nu} c_{\mu}^i c_{\nu}^i H_{\mu\nu}^0 + E_{\text{rep}} + \frac{1}{2} \sum_{\alpha\beta} \gamma_{\alpha\beta} \Delta q_{\alpha} \Delta q_{\beta} + \frac{1}{3} \sum_{\alpha\beta} \Gamma_{\alpha\beta} \Delta q_{\alpha}^2 \Delta q_{\beta} \quad (1)$$

where  $H_{\mu\nu}^0$  are the Hamiltonian matrix elements and  $c_{\mu}^i$  and  $c_{\nu}^i$  are the wave function expansion coefficients,  $E_{\text{rep}}$  accounts for short-range repulsive term, and  $\Delta q_{\alpha}$  and  $\Delta q_{\beta}$  are the charge fluctuation terms associated with atoms  $\alpha$  and  $\beta$ , respectively. The  $\gamma_{\alpha\beta}$  function is determined by

$$\gamma_{\alpha\beta} = \frac{1}{R_{\alpha\beta}} - S_{\alpha\beta} f_{\alpha\beta}$$

$$f_{\alpha\beta} = \begin{cases} \exp\left[-\left(\frac{U_{\alpha} + U_{\beta}}{2}\right)^{\zeta} R_{\alpha\beta}^2\right], & \text{if } (\alpha \text{ or } \beta = \text{H}) \\ 1, & \text{otherwise} \end{cases} \quad (2)$$

where  $S_{\alpha\beta}$  is an exponentially decaying short-range function. The damping function  $f_{\alpha\beta}$  is introduced to help describe hydrogen-bonding interactions, where  $U_{\alpha}$  and  $U_{\beta}$  are the atomic Hubbard parameters related to the chemical hardness of atoms  $\alpha$  and  $\beta$ , respectively. The parameter  $\zeta$  is determined by fitting to hydrogen bonding energies for select clusters from higher-level QM calculations.<sup>17</sup> The last term in eq 1 is a third order correction that was initially introduced with only the on-site third order term<sup>17</sup> but was recently implemented with the complete third order term.<sup>3</sup> The  $\Gamma_{\alpha\beta}$  describes derivatives of the  $\gamma$  function with respect to atomic charges. The introduction of this third order correction is suggested to improve the description of charged systems.<sup>3,17</sup>

In ref 7, a new parameter set named 3OB was designed such that both the electronic and repulsive potential parameters (appearing in the first and second terms in eq 1, respectively) are optimized for full third order SCC-DFTB calculations. In gas phase calculations this parameter set was shown to outperform the old MIO parameter set due to an improved geometry of nonbonded interactions and reduction of over-binding errors.<sup>7</sup> In the present work, we benchmark the newest, full third order SCC-DFTB method using the 3OB parameter set. The SCC-DFTB related parameters are taken from ref 7.

**2.2. LS2 QM/MM Simulation.** The LS2 system (shown in Figure 1) was constructed using the same protocol as described in detail in ref 15. A reduced system was composed of the LS2 channel with pore waters inside and a 10 Å-thick layer of equilibrated water molecules on either side of the channel, but with the lipid bilayer surrounding LS2 removed. Two layers of virtual atoms were added at the position of lipid head groups to prevent water molecules from entering the membrane region (see Figure 1). The virtual atoms had zero charge, Lennard-Jones (LJ) parameters of  $\sigma = 1.781797$  Å and  $\epsilon = 0.11$  kcal/mol, and were hexagonally close-packed with spacing of 1.95 Å. The parameters of the virtual atoms were chosen to minimize their effect on the pore water, while preventing water molecules from leaking into the lipid bilayer region. To maintain the integrity of the LS2 channel structure, harmonic position restraints with force constants of 1000 kJ/mol·Å<sup>2</sup> were applied to the  $C_{\alpha}$  atoms. These restraints were previously shown to maintain the channel geometry and pore water diffusion

constants of the realistic composite system.<sup>15</sup> The protein was described by the CHARMM22 force field<sup>18,19</sup> and the classical water molecules by the TIP3P<sup>20</sup> model modified for the CHARMM force field.

To equilibrate the system, initial velocities were assigned consistent with a temperature of 300 K that was then maintained with a Nosé–Hoover thermostat using a relaxation time constant of 0.1 ps for 10 ns of constant NVT simulation. The integration time step was 1 fs. The cutoff radius for LJ interactions was 12 Å employing a switching function starting at 10 Å. The cutoff radius for real space electrostatic interactions was 12 Å and the long-range electrostatics were treated by Particle–Particle Particle–Mesh (PPPM) method<sup>21</sup> with an accuracy threshold of  $10^{-4}$ .

To set up a protonated water wire inside the LS2 channel, an excess proton was placed near one of the channel waters, forming a classical hydronium cation parametrized consistently with the MS-EVB3 model.<sup>22</sup> A chloride counterion was added to the bulk water region to maintain charge neutrality. A harmonic potential with a 4 kcal/mol·Å<sup>2</sup> force constant was applied to the hydronium oxygen atom to restrain its *z* coordinate around *z* = −6.5 Å and *z* = −3.5 Å, coinciding with a minimum and a maximum in the previously calculated free energy profile for PT through the channel.<sup>13</sup> The protonated system was equilibrated for 1 ns at 300 K using the same settings as described above. All equilibration simulations were performed with the LAMMPS package (<http://lammps.sandia.gov>).<sup>23</sup>

The last snapshot of the MS-EVB3 equilibration was used as the initial structure for the QM/MM simulation. For the unprotonated LS2 system, the QM region included all of the channel water molecules (22–25 water molecules). For the protonated system, the QM region included all channel water molecules plus the excess proton. For the DFT/MM setup, the QM box size was 12 Å × 12 Å × 32 Å, with the *z* direction aligned with the channel axis. A quadratic confining wall potential was used to restrain the QM atoms within the QM box, with a wall skin thickness of 1 Å × 1 Å × 2.5 Å. The QM box size was chosen such that the quadratic wall potential did not affect the QM atoms for the majority of the simulation. The QM region was treated with several different density functionals under the Gaussian plane wave (GPW) scheme.<sup>24</sup> Two generalized gradient approximation (GGA) level exchange–correlation functionals were employed: the BLYP functional<sup>25,26</sup> with a empirical dispersion corrections<sup>27</sup> and the HCTH/120 functional<sup>28</sup> (hereafter denoted as BLYP-D and HCTH, respectively). In addition, the hybrid GGA level DFT method B3LYP<sup>29</sup> with a dispersion correction<sup>27</sup> (B3LYP-D) was employed to improve accuracy. For BLYP-D and HCTH, the Goedecker–Teter–Hutter (GTH) pseudopotentials<sup>30</sup> were used and the Kohn–Sham orbitals were expanded in the Gaussian TZV2P basis set. The electron density was expanded by auxiliary plane wave basis set up to 300 Ry. For B3LYP-D, GTH pseudopotentials for BLYP were used, and the wave function was expanded in the Gaussian DZVP basis set with an energy cutoff of 300 Ry for the plane wave basis set. The Gaussian Expansion of the Electrostatic Potential (GEEP) scheme was used to treat the QM/MM electrostatic coupling with periodic boundary conditions (PBCs),<sup>31,32</sup> and the spurious QM/QM periodic image interactions were decoupled as described in ref 33. The QM/MM van der Waals (vdW) interactions were described by the CHARMM22 force field Lennard-Jones (LJ) parameters. The motion of nuclei was

integrated using a time step of 0.5 fs, and the wave function was optimized to the Born–Oppenheimer surface by an orbital transformation method<sup>34</sup> with a convergence criterion of  $10^{-6}$ . All DFT/MM simulations were run using the CP2K package.<sup>35</sup>

For the SCC-DFTB/MM setup, the QM atoms were chosen in the same way as DFT/MM and planar restraining potentials were used to prevent the boundary QM atoms from diffusing out of the channel. Again, the QM atoms within the boundary defined by the planes were not affected. The point charge based Ewald summation was used to treat QM/MM electrostatic coupling under PBCs.<sup>16</sup> Just as for the DFT/MM simulations, the SCC-DFTB/MM vdW interactions were described by the CHARMM22 force field LJ parameters. The time step was set as 0.5 fs, and the SCC-DFTB convergence criterion of  $10^{-8}$  was used. The SCC-DFTB/MM simulations were carried out using the CHARMM simulation package.<sup>36</sup>

In previous studies, the PT free energy profile through the LS2 channel features several local minima separated by energy barriers that are several times that of the thermal energy, thus impeding the free translocation of the excess proton.<sup>13</sup> In order to make a statistically meaningful comparison between SCC-DFTB and DFT methods for the PT properties within a limited simulation time (~100 ps), we chose to enhance the sampling of the excess proton in two regions inside the LS2 channel (one wider and one narrower region). In particular, the *z* position was restrained with a harmonic potential around *z* = −6.5 Å (Figure 2), which corresponds to a wide region in the channel where the complete first solvation shell of the excess proton can be accommodated and a minimum in the PT free energy profile was previously reported (Figure 2 in ref <sup>13</sup>), and *z* = −3.5 Å, corresponding to a narrow channel region and a barrier top in the PT free energy profile.

The charge defect associated with the excess proton was tracked via the center of excess charge (CEC) defined in this work as<sup>37</sup>

$$\vec{\zeta} = \sum_{i=1}^{N_H} \vec{r}^{H_i} - \sum_{j=1}^{N_O} w^O \vec{r}^{O_j} - \sum_{i=1}^{N_H} \sum_{j=1}^{N_O} f_{sw}(d_{O_i H_j}) (\vec{r}^{H_i} - \vec{r}^{O_j}) \quad (3)$$

where the “O” and “H” denotes oxygen atoms and hydrogen atoms in the QM region, the weighting factor  $w^O$ ’s are set to 2,  $d_{O_i H_j}$  is the distance between atom  $O_j$  and atom  $H_i$ , and  $f_{sw}(d_{O_i H_j}) = 1/(1 + \exp[(d_{O_i H_j} - r_{sw})/d_{sw}])$  is the switching function describing the coordination number of  $H_i$  to  $O_j$ , with the parameters chosen as  $d_{sw} = 0.03$  Å,  $r_{sw} = 0.13$  Å.<sup>37</sup> This excess proton CEC definition has been shown to adequately locate the position of the excess proton charge defect in previous QM/MM simulations of biological PT channels.<sup>11,37</sup> This quantity will be referred to often in the following discussion so the readers should take note of this acronym and its definition.

Following 200 steps of steepest descent geometry minimization, the systems were heated up and the temperature then maintained at 300 K using a Nosé–Hoover thermostat with a relaxation time constant of 0.1 ps for all of the methods. For the all of the methods, both restrained and unrestrained simulations of the protonated LS2 channel were run, with the latter starting from the last snapshot of the corresponding method’s restrained simulation. All the QM/MM simulations were equilibrated for at least 30 ps and run for another 70–100 ps in the constant NVT ensemble.



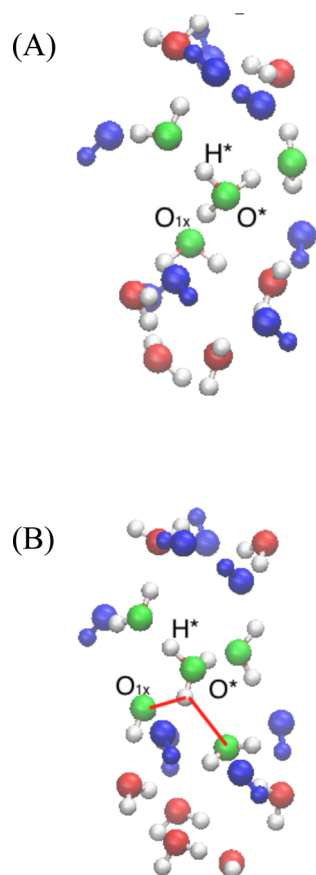


**Figure 2.** Snapshots of protonated water wire in LS2 with excess proton CEC restrained at  $z = -6.5$  Å from (A) BLYP-D simulation (B) SCC-DFTB simulation. The serine residues are colored in blue, the most hydronium-like oxygen  $O^*$  and the water oxygens within 3 Å of  $O^*$  are colored in green, and the rest of the water oxygens are colored in red. One of the hydrogens closest to the  $O^*$  is shown by  $H^*$  and the next closest oxygen in the special pair,  $O_{1x}$  is also shown in panel A. Notice the oversolvation of SCC-DFTB  $O^*$  and the bifurcated hydrogen bond indicated by the red lines in panel B.

**2.3. Carbon Nanotube QM/MM Simulation.** A (8,8) single-wall carbon nanotube (CNT) of length 29.47 Å was first solvated in a large box of equilibrated TIP3P water. The LJ parameters for carbon atoms were  $\sigma = 3.40$  Å and  $\epsilon = 0.086$  kcal/mol, corresponding to the  $sp^2$  carbon atoms in the AMBER force field.<sup>38</sup> All the carbon atoms were fixed. The cutoffs for LJ and real space electrostatic interactions were 10 Å, employing switching function starting at 8 Å for the LJ interactions. To equilibrate the system, initial velocities were assigned to 300 K followed by 20 ps of constant NVT and then 2 ns of constant NPT equilibration. On average 38 water molecules resided in the CNT during the NPT equilibration. One snapshot was taken from the last 10% of the equilibration run, in which 38 water molecules were inside the CNT, and water molecules outside the CNT were removed. Then, the simulation box was set up with PBC of  $20$  Å  $\times$   $20$  Å  $\times$   $29.47$  Å, and the longest dimension of simulation box was aligned with tube axis to create an infinitely long CNT. The system was equilibrated at 300 K using Nosé–Hoover thermostat for 1 ns. One excess proton was then added near one water molecule, and the equilibration was continued for 1 ns using the same classical hydronium model as used in the LS2 equilibration. All

the equilibration simulations were again carried out with LAMMPS.

The last snapshot of equilibration was used to construct the QM/MM simulation. The QM atoms were chosen to be all the water molecules and the excess proton. Following 40 ps of constant NVT simulation at 300 K using a Nosé–Hoover thermostat, the production constant NVE runs were continued for at least 80 ps. The DFT/MM simulations were run with the BLYP-D and HCTH functionals. The QM/MM settings were the same as those used in the LS2 channel, except that the energy cutoff for plane wave basis set was increased to 360 Ry and the convergence criterion was decreased to  $10^{-7}$  to better conserve total energy. For the SCC-DFTB/MM simulations, the convergence criterion was  $10^{-8}$ . For all QM/MM simulations, the motion of nuclei was integrated using a time step of 0.5 fs.

## RESULTS

**3.1. Water Structure and Dynamics in the LS2 Channel.** The water molecules filling the LS2 channel make hydrogen bonds with one another and with pore lining serine side chains, resulting in a continuous hydrogen-bonded water wire across the entire channel.<sup>15,39</sup> It is beneficial to first investigate the properties of pure water in the LS2 channel. The BLYP functional with dispersion corrections (BLYP-D) and HCTH/120 functional are chosen as the benchmark QM methods because both methods were shown to reduce the excessive structuring and sluggish dynamics of bulk water predicted by the BLYP functional.<sup>40–44</sup> These functionals were in turn benchmarked by simulations using the arguably more accurate B3LYP functional with dispersion corrections (B3LYP-D). To save computational cost, B3LYP-D was combined with GTH pseudopotentials for BLYP and the DZVP basis set. We note that B3LYP should generally be used with a large basis set augmented by diffuse functions in order to guarantee a highly accurate hydrogen bond description.<sup>45</sup> Although this was not computationally feasible, the B3LYP-D employed in our QM/MM simulations still provide more accurate forces and energies than GGA level DFT methods. (See Supporting Information)

In the following, the water oxygen, water hydrogen, and serine oxygen atoms will be denoted as  $O_w$ ,  $H_w$ , and  $O_s$ , respectively. To probe the structural properties of the water within the channel, radial distribution functions (RDFs) were calculated and normalized to bulk water density. From the  $O_w$ – $O_w$  RDF (Figure 3A), it is apparent that SCC-DFTB predicts a more pronounced first peak. The coordination number, obtained by integrating over the first peak, is larger for SCC-DFTB due to a more compact and dense first solvation shell. In addition, the second peak in the  $O_w$ – $O_w$  RDF and the density depletion region between second and third peaks in the  $O_w$ – $H_w$  RDF (Figure 3B) are less pronounced for SCC-DFTB than for the DFT methods, which corresponds to a second solvation shell water encroaching on the first solvation shell. This suggests that the water wire predicted by SCC-DFTB is less ordered inside the LS2 channel. In line with this observation, SCC-DFTB predicts less distinct peaks and valleys in the pore water density profile along the  $z$  axis (Figure 4) compared to both DFT methods, indicating that the water molecules deep in the pore region ( $-10$  Å to  $10$  Å) are more mobile.

The decreased structure in the LS2 channel water could be caused by weaker water–water hydrogen bonds in SCC-DFTB compared to those in the DFT methods. To quantitatively

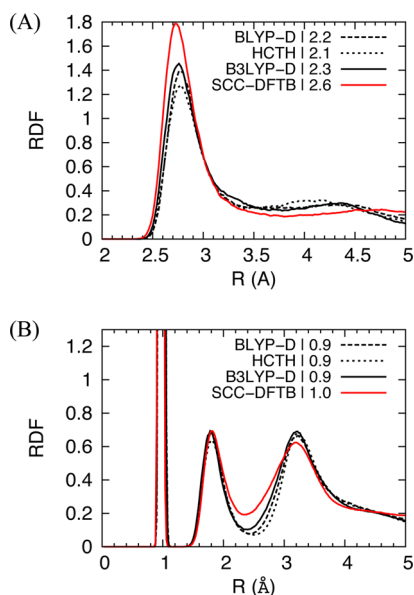


**Figure 3.** RDFs of (A)  $O_w-O_w$  and (B)  $O_w-H_w$  in the LS2 channel filled with water and no excess proton. The coordination numbers, indicated in the legend, are larger for the SCC-DFTB method due to less structured 2nd shell waters encroaching on the 1st solvation shell.

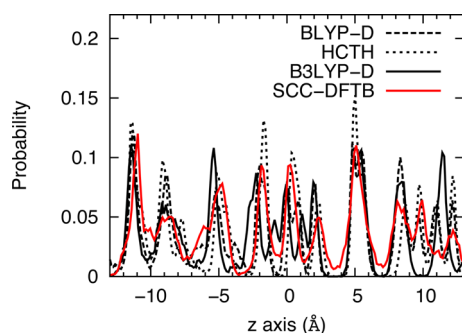


**Figure 4.** Distribution of the pore water oxygen atoms along the  $z$  axis of the unprotonated LS2 channel. The decreased peaks and valleys for the SCC-DFTB results indicate more mobile water within the channel.

investigate the hydrogen bond properties, we define the water–water hydrogen bond as when the  $O_w-O_w$  separation is less than 3.5 Å (corresponding to the location of the first minimum in the  $O_w-O_w$  RDF) and the  $H_w-O_w-O_w$  angle is less than  $30^\circ$ .<sup>46,47</sup> The number of water–water hydrogen bonds each water molecule makes is averaged over the entire 90 ps production trajectory and listed in Table 1. It is observed that the channel water described by SCC-DFTB forms fewer hydrogen bonds than those described by the DFT methods, which are in close agreement with each other. To compare the longevity of the hydrogen bonds, we calculated the continuous

**Table 1.** Averaged Number of Hydrogen Bonds Per Water Molecule in the LS2 Channel As a Function of QM/MM Methodology

methods	water–water hydrogen bond	serine–water hydrogen bond
BLYP-D	$1.64 \pm 0.03$	$1.14 \pm 0.01$
HCTH	$1.66 \pm 0.02$	$1.17 \pm 0.02$
B3LYP-D	$1.60 \pm 0.02$	$1.17 \pm 0.02$
SCC-DFTB	$1.51 \pm 0.01$	$1.06 \pm 0.02$

hydrogen bond time correlation function  $C_c(t) = \langle h(0) \cdot H(t) \rangle / \langle h \rangle$ , where  $h(t)$  is unity when a tagged pair of atoms are hydrogen bonded at time  $t$ , and zero otherwise.  $H(t)$  is defined as unity when the tagged pair of atoms is continuously hydrogen bonded from time 0 to time  $t$ , and zero otherwise. A semilog plot of  $C_c(t)$  is shown in Figure 5A. The continuous

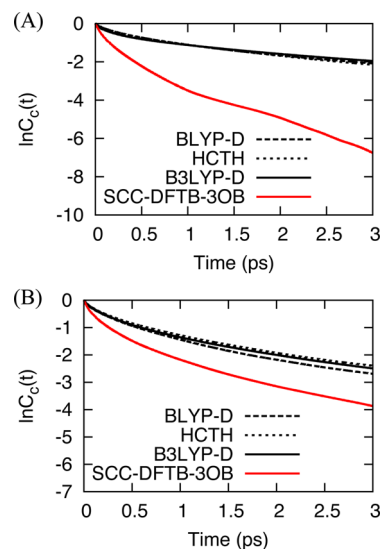


**Figure 5.** Semilog plot of continuous hydrogen bond time correlation function for the (A) water–water and (B) water–serine hydrogen bonds. The faster decay of time-correlation functions reflects weaker hydrogen bonds described by SCC-DFTB compared to the DFT methods.

hydrogen bond time correlation functions are then fit to the sum of 3 exponential functions, and the average relaxation time is estimated by the amplitude-averaged relaxation time,<sup>48,49</sup> as summarized in Table 2. It is observed that SCC-DFTB

**Table 2.** Average Water–Water, Water–Serine Hydrogen Bond Relaxation Time, and Orientational Correlation Time in the LS2 Channel As a Function of QM/MM Methodology

method	water–water hydrogen bond relaxation time (ps)	water–serine hydrogen bond relaxation time (ps)	water orientational correlation time (ps)
BLYP-D	1.26	0.86	24
HCTH	1.20	1.03	28
B3LYP-D	1.38	0.93	23
SCC-DFTB	0.21	0.42	7

produces a shorter hydrogen bond relaxation time compared to the DFT methods, again confirming shorter (and likely weaker) water–water hydrogen bond interactions.

The interaction between water and the serine side chains also plays an important role in shaping the structure and slowing down the dynamics of water inside the LS2 channel.<sup>39</sup> The  $O_w-O_s$  RDF (Figure 6) reveals that SCC-DFTB fails to reproduce the DFT density depletion region after the first peak and the presence of a second peak. Similar to the situation with water–water interactions, the less ordered structure revealed in the SCC-DFTB RDF reflects weaker interactions between water and serine side chains. With the water–serine hydrogen bond defined using the same distance and angle cutoff as the water–water hydrogen bond (described above), we calculated

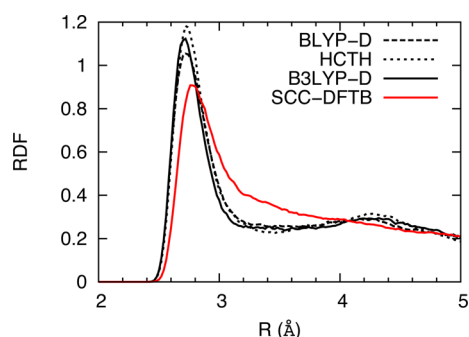


**Figure 6.** RDF of  $O_w-O_s$  in the LS2 channel filled with water and no excess proton. The less structured RDF produced by SCC-DFTB indicates weaker water–serine interactions due to weaker and fewer hydrogen bonds.

the average number of water–serine hydrogen bonds each water makes (listed in Table 1) and the continuous hydrogen bond correlation function together with the hydrogen bond relaxation time (Figure 5B and Table 2). The fewer number of water–serine hydrogen bonds with each water molecule and the faster relaxation of those hydrogen bonds for SCC-DFTB suggest that the weaker water–serine interaction results from fewer and weaker hydrogen bonds.

The consequence of weaker water–water and water–serine interactions is a less structured water wire inside the LS2 channel with accelerated orientational dynamics in the SCC-DFTB simulations. To probe the orientational dynamics, the second rank orientation time-correlation function  $C_2(t) = \langle P_2(\mathbf{u}(0) \cdot \mathbf{u}(t)) \rangle / \langle P_2(\mathbf{u}(0) \cdot \mathbf{u}(0)) \rangle$  was calculated, where  $\mathbf{u}$  is the unit vector in the direction of one of the O–H bonds in water and  $P_2$  is the second order Legendre polynomial. The last 30% of  $C_2(t)$  are summarized in Table 2. It is found that the SCC-DFTB method predicts water reorientation much faster than the two DFT methods, again indicating more dynamic and disordered water in the LS2 channel.

Overall, SCC-DFTB predicts an overcoordinated and more disordered water structure featuring faster dynamics of water molecules compared to the DFT methods. These differences in the structural and dynamical properties of unprotonated water are in turn linked to differences in the structure and dynamics of PT, as will be discussed.

**3.2. Proton Solvation and Transport in a Wider Region of the LS2 Channel.** In the following the hydronium oxygen, the three closest hydrogen atoms to that oxygen, and the next closest oxygen atom will be denoted as  $O^*$ ,  $H^*$ , and  $O_{1x}$ , respectively (see Figure 2A). The  $O_{1x}$  is the so-called “special pair” oxygen that is forming an especially short strong hydrogen bond with the hydronium at that instant in time. Proton transfer often, but not always, occurs along this special pair coordinate.<sup>50</sup> From the RDFs of  $O^*-O_w$  and  $O_{1x}-O$  ( $O$  here denotes  $O^*$  and  $O_w$ ) (Figure 7A and B), it is apparent that SCC-DFTB predicts an overcoordinated hydronium oxygen, with a coordination number of 3.56 compared to those predicted by the DFT methods (all  $\sim 3$ ). Also, the solvation shell around the  $O^*$  is less structured in the SCC-DFTB simulations than the DFT counterparts. Where the DFT methods predict a distinct density depletion after the first peak of the  $O^*-O_w$  RDF (at separation distance of 2.8 Å corresponding to the boundary of the first solvation shell), SCC-DFTB predicts a density decay region that extends beyond 3.4 Å. The overcoordination of  $O^*$  and lack of distinct density depletion beyond the first solvation shell suggests that second solvation shell water molecules penetrate into the first, making the solvation structure less ordered compared to DFT simulations. In fact, it is observed that in DFT simulations the hydronium is consistently coordinated by three first solvation shell water molecules, forming a stable  $H_3O_4^+$  Eigen complex, which is further stabilized by hydrogen bond interactions with nearby serine side chains and second solvation shell water molecules (Figure 2A). In contrast, the SCC-DFTB method predicts an overcoordinated hydronium due to a second solvation shell water molecule frequently entering the 3 Å range of  $O^*$ , leading to a *bifurcated hydrogen bond* (one hydrogen

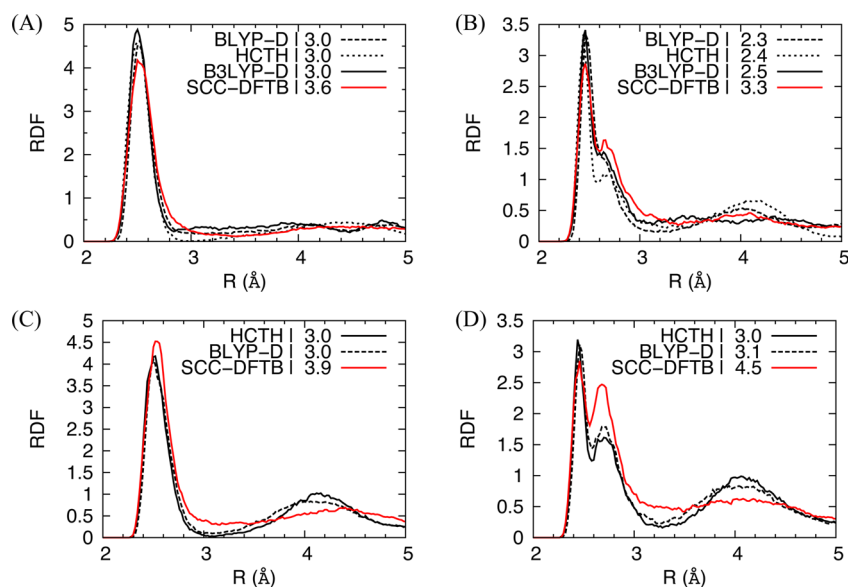


**Figure 7.** RDFs of (A)  $O^*-O_w$  and (B)  $O_{1x}-O$ , where  $O$  includes both  $O^*$  and  $O_w$ , in protonated LS2. RDFs of (C)  $O^*-O_w$  and (D)  $O_{1x}-O$ , where  $O$  includes both  $O^*$  and  $O_w$ , in protonated water filled CNT. Coordination numbers are indicated in the legend. SCC-DFTB predicts an overcoordinated excess proton and less structured solvation complex compared to the DFT methods.

coordinated to two water oxygens) and disrupting the Eigen complex solvation structure (Figure 2B). As will be discussed, the SCC-DFTB hydronium is also directly coordinated to serine side chains much of the time, further increasing its overcoordination. In addition, the SCC-DFTB first solvation shell waters are also overcoordinated as indicated by the large coordination number shown in the RDF's of  $O_{1x}$ -O (Figure 7B), which is in line with this method's tendency to overcoordinate water as discussed in section 3.1.

The overcoordinated excess proton structure described by SCC-DFTB leads to an abnormal hydrogen bond network around the excess proton. To illustrate this, the RDF of  $H^*-O_w$ , where  $H^*$  is any of the three hydrogens bound to  $O^*$ , is plotted for LS2 (Figure 8A). The absence of density depletion

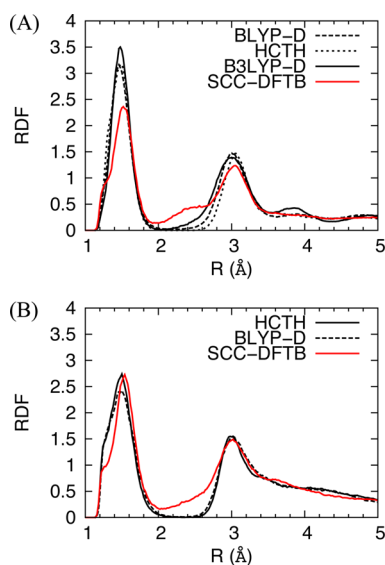


**Figure 8.** (A) RDF of  $H^*-O_w$  in the protonated LS2, (B) RDF of  $H^*-O_w$  in water filled protonated CNT. The absence of density depletion in the distance region 2–2.5 Å in the SCC-DFTB results reflects the encroaching 2nd solvation shell water and bifurcated hydrogen bond donated by the hydronium.

in the region 2–2.5 Å in the SCC-DFTB results reflects the encroaching second solvation shell water and bifurcated hydrogen bond donated by the hydronium. This observation is perhaps even more clear in Figure 9A, which shows the distribution of first and second closest water oxygens to each  $H^*$ . Clearly, there is an overlap region between the two distributions for SCC-DFTB simulations, which is absent in the DFT results. The overlap is a consequence of the SCC-DFTB method not localizing the first solvation shell water molecules, making it more likely to form a bifurcated hydrogen bond with two waters in its first solvation shell (see Figure 2B).

Although SCC-DFTB results in an increased probability of forming a bifurcated hydrogen bond, the water penetrating the first solvation shell is not hydrogen bonded to the  $O^*-H^*$  at all for a significant amount of time. Figure 10A shows the distribution of the distance between  $O^*$  and the nearest water oxygen atoms that are not hydrogen bonded to it. In the SCC-DFTB simulations, for both the LS2 and CNT channels, an unphysical configuration is frequently observed where a water molecule within the range of first solvation shell (2.8 Å of  $O^*$ ) is not hydrogen bonded to it. More surprisingly, the  $O_w$  not hydrogen bonded to or forming a bifurcated hydrogen bond

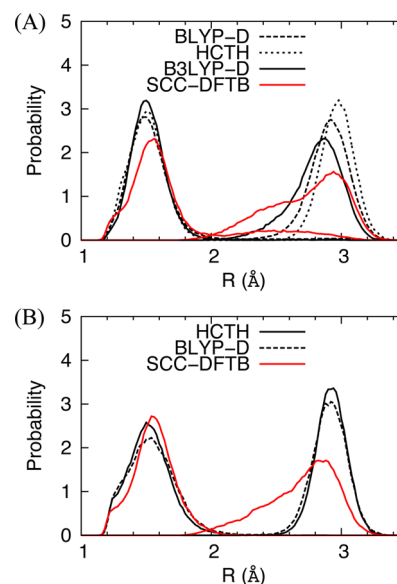


**Figure 9.** Distribution of  $H^*-O_w$  distances in protonated (A) LS2 channel and (B) CNT. The first and second peaks correspond to the closest and second closest  $O_w$  to  $H^*$ . The overlap of the two peaks in the SCC-DFTB simulation suggests that hydrogen bonding around the excess proton is too weak to localize the position of its first solvation shell water molecules, making it more likely to form a bifurcated hydrogen bond with two waters in its first solvation shell.

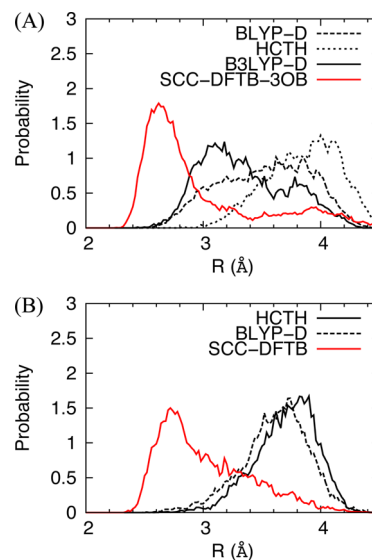


**Figure 10.** Distribution of  $O^*-O$  distance, where O is the closest atom not hydrogen bonded to  $O^*$  in the (A) protonated LS2 channel and (B) CNT. The noticeable peak before 2.8 Å produced by SCC-DFTB indicates that on average some first solvation shell water molecules are not hydrogen bonded to the hydronium, which perturbs the “special pair dance” dynamics in the resting state of PT (see main text).

with  $O^*$  can even belong to the closest water molecule for a significant portion of the simulation time. It has been shown that in a bulk aqueous system during the long intervals between PT events (aka non-PT intervals), the closest oxygen to  $O^*$  ( $O_{1x}$ ) switches between the 3 surrounding water oxygens in the Eigen complex, resulting in a “special pair dance” mechanism.<sup>50</sup> The existence of a penetrating water molecule that is closest to  $O^*$  but not hydrogen bonded to it will alter PT dynamics and



limit SCC-DFTB's ability to correctly capture the special pair dance dynamics in the LS2 channel. To probe this, we calculated the average number of distinct  $O_w$  atoms that have been  $O_{1x}$  during non-PT intervals. As shown in Figure 11 the

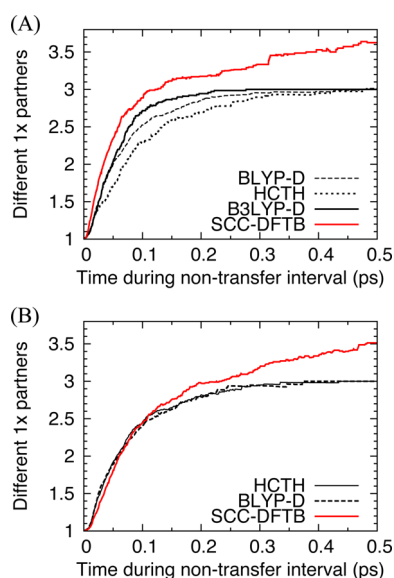


**Figure 11.** Average number of different  $O_{1x}$  partners to  $O^*$  as a function of time during nontransfer intervals for the (A) LS2 and (B) CNT. The SCC-DFTB curve fails to level off and indicates that it does not reproduce the “special pair dance” behavior seen from the DFT results.

DFT simulations show a mechanism in which  $O_{1x}$  rotates among the three hydrogen bond accepting waters around  $O^*$ .<sup>50</sup> Correspondingly, the number of different water oxygens that have once been  $O_{1x}$  levels off at 3 in 0.4 ps. However, the SCC-DFTB method predicts more than three  $O_{1x}$  water molecules exhibiting this behavior. Moreover, the curve shows no sign of leveling off near 0.5 ps. In the SCC-DFTB simulations, the  $O_w$  chosen as special partner,  $O_{1x}$ , sometimes belongs to a water molecule accepting a hydrogen bond from  $O^*$ , while at other times it belongs to the penetrating water molecule not hydrogen bonded to or forming one of the bifurcated hydrogen bonds with  $O^*$ . These situations interchange frequently resulting in a qualitatively different dynamical picture than that predicted by DFT.

To further illustrate the weak hydrogen bond around  $O^*$  in SCC-DFTB from a dynamical point of view, we applied the same analysis of average hydrogen bond relaxation times as was shown for the unprotonated water in LS2. Table 3 compares the relaxation times of hydrogen bonds within 4 Å of the excess proton CEC (defined in section 2.2) for different methods in

**Table 3.** Average Hydrogen Bond Relaxation Time for Hydrogen Bond Around 4 Å of Excess Proton CEC in the LS2 Channel and CNT as a Function of QM/MM Methodology

method	LS2 hydrogen bond relaxation time (ps)	CNT hydrogen bond relaxation time (ps)
BLYP-D	17.3	13.7
HCTH	19.8	10.0
B3LYP-D	11.2	NA
SCC-DFTB	1.8	1.4

both the LS2 and CNT systems. Not only is the SCC-DFTB hydrogen bond relaxation time much shorter than those predicted by the DFT methods, but the differences between SCC-DFTB and the DFT methods are much larger than those found for the unprotonated situation. This suggests that the effect of charge defect delocalization in enhancing hydrogen bond strength around the excess proton CEC is relatively weaker for SCC-DFTB than for the DFT methods. Thus, improving the description of hydrogen bond around the hydrated excess proton needs to be addressed in future SCC-DFTB developments.

Overall, compared to the arguably more accurate DFT approaches, the SCC-DFTB method predicts the incorrect solvation structure of water and the excess proton, weak water–water and water–serine hydrogen bond interactions, a bifurcated hydrogen bond donated by the hydronium-like oxygen  $O^*$ , and an unphysical special pair dynamics pattern related to the weak hydrogen bonds around the excess proton CEC. These all lead to qualitatively different PT dynamics in the LS2 and CNT channels. The PT dynamics can also be described by the time evolution of the excess proton CEC  $z$  coordinate after the quadratic restraints on it are released, as shown in Figure 12. For the DFT methods, the excess charge is stabilized in the form of an Eigen complex, which is further stabilized by the surrounding water and serine residues. During more than 70 ps of simulation the excess proton CEC  $z$

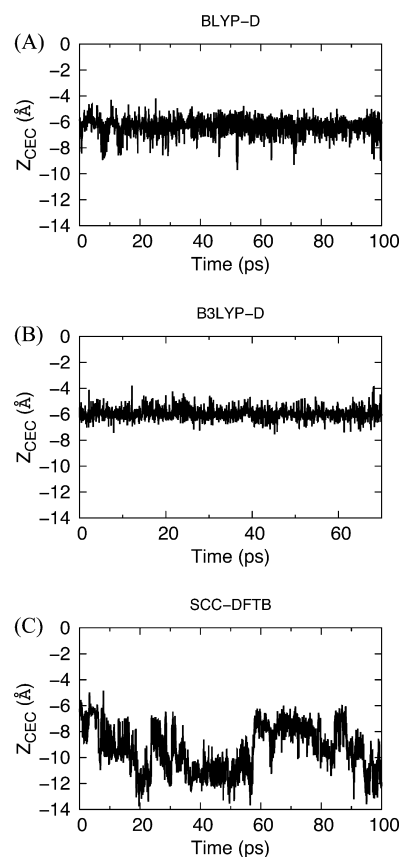


**Figure 12.**  $Z$  coordinate of the excess proton CEC as a function of time for unconstrained simulations using the (A) BLYP-D, (B) B3LYP-D, and (C) SCC-DFTB methods. The SCC-DFTB simulations show deviations as far as 6 Å from the previous reference point of the restraint, which indicates that the excess proton is not stabilized in an Eigen complex.



coordinate fluctuates around  $z = -6 \text{ \AA}$ , which is close to the reference point where the restraint was added. This suggests that the chosen region in the LS2 channel corresponds to a distinct free energy minimum in the free energy profile described by the DFT methods, in agreement with the previous MS-EVB result.<sup>13</sup> In sharp contrast, the excess proton CEC  $z$  coordinate in the SCC-DFTB simulations deviates as far as  $6 \text{ \AA}$  from the previous reference point, which indicates that the excess proton is not stabilized in an Eigen complex. It hops around the overcoordinated, less ordered, and loosely bound solvation shell in an unpredictable manner and gradually hops away from the region where it was originally restrained. This can be attributed to the combined effect of weaker water–water and water–serine interactions, the overcoordinated hydronium  $\text{O}^*$ , the weak and sometimes bifurcated hydrogen bond around the excess proton CEC, as well as the unphysical  $\text{O}_{1x}$  switching events.

The tendency for SCC-DFTB to yield irregular excess proton solvation and transport remains even when the excess proton CEC motion is more trapped in the constrained simulations. In the constrained simulation SCC-DFTB predicts an  $\text{O}^*-\text{O}_s$  RDF featuring a spurious first peak within  $3 \text{ \AA}$  (Figure 13A).

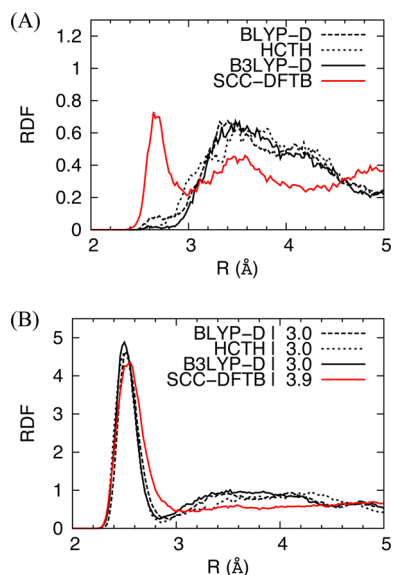


**Figure 13.** (A) RDF of  $\text{O}^*-\text{O}_s$  between the excess proton complex and serines in the protonated LS2 channel. The first peak predicted by SCC-DFTB method reveals that the hydronium is directly hydrogen bonded to serine side chain hydroxyl groups for significant amounts of the simulation. (B) The RDF of  $\text{O}^*-\text{O}$ , where  $\text{O}$  includes both  $\text{O}_w$  and  $\text{O}_s$ . Compared with Figure 7A, the coordination numbers indicate that the serine side chains exacerbates the overcoordination issue of  $\text{O}^*$  in SCC-DFTB simulations.

This is caused by  $\text{O}^*$  being directly hydrogen bonded to serine side chain hydroxyl groups for significant amounts of the simulation, something that is not observed in the DFT simulations. It is important to note that this close interaction between serine side chain oxygen atoms and the hydronium further exacerbates the overcoordination issue already caused by excessive water molecules around the SCC-DFTB hydronium in the LS2 channel. To illustrate this, the RDF of  $\text{O}^*-\text{O}$ , where  $\text{O}$  denotes both  $\text{O}_w$  and  $\text{O}_s$ , is plotted in Figure 13B. Comparing the coordination numbers in Figure 7A and Figure 13B (3.6 versus 3.9) demonstrates that the overcoordination

around the excess proton is more pronounced when the serine oxygen atoms are included. Figure 13B shows that SCC-DFTB predicts an  $\text{O}^*$  coordinated by four oxygen atoms, in contrast to three as predicted by the DFT methods. This observation is revealing because it shows that the SCC-DFTB hydronium  $\text{O}^*$  favors an oxygen coordination number of 4. When its water coordination number is less than 4 in a confined environment (as shown in Figure 7A), the serine side chain oxygen atoms tend to further coordinate  $\text{O}^*$  to saturate its solvation shell if allowed by local geometry.

**3.3. Proton Solvation and Transport in a Narrower Region of the LS2 Channel.** Clearly, narrow channel regions also play an important role in PT processes, as previously demonstrated for the LS2 channel.<sup>13,15</sup> It is, therefore, both important and instructive to also study the proton solvation structure and transport mechanism in a narrower region ( $z = -3.5 \text{ \AA}$ ) close to the top of a barrier in a previously reported LS2 PMF.<sup>13</sup> As shown in Figure 14A and B, the DFT methods predict a  $\text{H}_7\text{O}_3^+$  solvation structure of the excess proton, that is, the hydronium solvated by two nearby water molecules and one serine hydroxyl group. In contrast, the SCC-DFTB method predicts an overcoordinated excess proton, just as it did in the wider region of the LS2 channel, with an additional water and

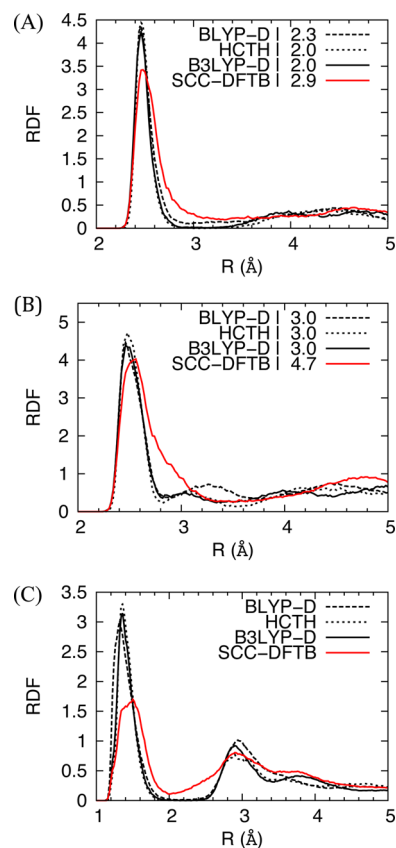


**Figure 14.** RDFs of  $\text{O}^*-\text{O}_w$  (A),  $\text{O}^*-\text{O}$  where  $\text{O}$  includes both  $\text{O}_w$  and  $\text{O}_s$  (B), and  $\text{H}^*-\text{O}_w$  (C) in a narrower region of protonated LS2 channel. The coordination numbers in panels A and B indicate that SCC-DFTB's overcoordination of  $\text{O}^*$  remains in the narrow region of the channel. The absence of density depletion in panel C (around  $2-2.5 \text{ \AA}$ ) in the SCC-DFTB results reflects the encroaching 2nd solvation shell water and bifurcated hydrogen bond donated by the hydronium ion are very similar to the case of the wider region (compare to Figure 8A).

serine hydroxyl in the first solvation shell. Also similar to the wider region, the absence of density depletion (around 2.0–2.5 Å in Figure 14C) in the SCC-DFTB results reflects a bifurcated hydrogen bond being donated by the hydronium. Therefore, the SCC-DFTB method displays similar defects in a more confined local environment. More results for the narrower region of the protonated LS2 channel can be found in the Supporting Information.

**3.4. Proton Solvation and Transport in (8,8) Single-Wall Carbon Nanotube.** The QM/MM electrostatic coupling scheme employed in the current work follows that of ref 16. The electrostatic interaction between SCC-DFTB atoms and MM atoms are calculated based on point charges. The point charges on QM atoms are the Mulliken charges  $\Delta q_a$  defined in the SCC-DFTB energy expression (eq 1). In the recent work of Hou et al.,<sup>51</sup> a new QM/MM coupling scheme was implemented for SCC-DFTB/MM, which takes into account the finite size of QM and MM charge distributions by using a Klopman-Ohno functional form for the QM/MM electrostatic coupling. The new SCC-DFTB/MM coupling scheme improves the short-range QM/MM interactions when the QM atoms are highly charged. In the LS2 channel, some of the QM atoms (the excess proton and solvating water molecules) are positively charged and are close to the serine side chains described by MM. In order to test whether the inaccuracies of the SCC-DFTB/MM LS2 simulations described above are a result of the original point charge based electrostatic coupling scheme,<sup>16</sup> a hydrophobic proton channel system was created from a (8,8) single-wall carbon nanotube (CNT) filled with water molecules and one excess proton. In this system the QM and MM atoms only interact via the same LJ potential for all the methods under comparison (see section 2.3). The effective pore radius of the CNT ( $\sim 4$  Å) is comparable to the wide region of the LS2 channel, accommodating one complete solvation shell around the hydronium  $O^+$  (i.e., the  $H_9O_4^+$  Eigen complex). Similar properties were calculated for the CNT as were for the LS2 channel, and are plotted in Figure 7 (C), (D), and Figures 8–11 (B). These results reveal that the SCC-DFTB inaccuracies discussed above for LS2 remain in the CNT, including the overcoordinated excess proton, weak hydrogen bond around the excess proton CEC, and PT dynamics at odds with the DFT results. Therefore, the inaccurate description of PT in the LS2 channel by SCC-DFTB/MM should not be attributed to using an approximate electrostatic coupling scheme but rather to inherent limitations of SCC-DFTB method itself.

## CONCLUSIONS

This benchmark study has shown that the SCC-DFTB method provides qualitatively different behavior for the solvation and transport of an excess proton in the LS2 channel. These differences, when compared to more exact DFT methods, which the SCC-DFTB approach is meant to approximate, include a less ordered water structure, an overcoordinated excess proton, weak hydrogen bonding around the excess proton CEC, and altered PT dynamics. These differences are also seen for the hydrated excess proton in a carbon nanotube involving only van der Waals interactions between QM and MM atoms, verifying that the SCC-DFTB inaccuracies relative to DFT in the LS2 channel result from the semiempirical QM method itself, rather than the QM/MM electrostatic coupling scheme. In addition, SCC-DFTB is shown to predict higher local water density in channel environments, similar to that

which has been shown in a previous study to cause clearly unphysical large pockets of vacuum in SCC-DFTB simulations of bulk aqueous systems.<sup>4,5</sup> The less accurate descriptions of water and the hydrated excess proton results in qualitatively and quantitatively different structural and dynamical properties for PT in confined channel environments, calling into question the ability of the current SCC-DFTB method to accurately simulate excess proton transport in realistic biomolecular systems. At the same time, the presented results provide an important set of benchmarks by which the method can potentially be improved in the future to bring it more in line with more accurate, but more computationally costly, DFT-based QM/MM methods.

## ASSOCIATED CONTENT

### Supporting Information

Comparison of the presented results to those of the multistate empirical valence bond (MS-EVB) method, along with additional results on the narrower region of the LS2 channel and a comparison of the BLYP3-D forces and energies with GGA level DFT. This material is available free of charge via the Internet at <http://pubs.acs.org>.

## AUTHOR INFORMATION

### Corresponding Author

\*E-mail: [gavoth@uchicago.edu](mailto:gavoth@uchicago.edu). Fax: 773-795-9106. Phone: 773-702-9092.

### Notes

The authors declare no competing financial interest.

## ACKNOWLEDGMENTS

This research was supported by the National Institutes of Health (NIH grant R01 GM053148).

## REFERENCES

- (1) Elstner, M.; Porezag, D.; Jungnickel, G.; Elsner, J.; Haugk, M.; Frauenheim, T.; Suhai, S.; Seifert, G. Self-consistent-charge density-functional tight-binding method for simulations of complex materials properties. *Phys. Rev. B* **1998**, *58*, 7260–7268.
- (2) Elstner, M. The SCC-DFTB method and its application to biological systems. *Theor. Chem. Acc.* **2006**, *116*, 316–325.
- (3) Gaus, M.; Cui, Q. A.; Elstner, M. DFTB3: Extension of the self-consistent-charge density-functional tight-binding method (SCC-DFTB). *J. Chem. Theory Comput.* **2011**, *7*, 931–948.
- (4) Maupin, C. M.; Aradi, B.; Voth, G. A. The self-consistent charge density functional tight binding method applied to liquid water and the hydrated excess proton: Benchmark simulations. *J. Phys. Chem. B* **2010**, *114*, 6922–6931.
- (5) Choi, T. H.; Liang, R.; Maupin, C. M.; Voth, G. A. Application of the SCC-DFTB method to hydroxide water clusters and aqueous hydroxide solutions. *J. Phys. Chem. B* **2013**, *117*, 5165–5179.
- (6) Goyal, P.; Elstner, M.; Cui, Q. Application of the SCC-DFTB method to neutral and protonated water clusters and bulk water. *J. Phys. Chem. B* **2011**, *115*, 6790–6805.
- (7) Gaus, M.; Goetz, A.; Elstner, M. Parametrization and benchmark of DFTB3 for organic molecules. *J. Chem. Theory Comput.* **2013**, *9*, 338–354.
- (8) Petraglia, R.; Corminboeuf, C. A caveat on SCC-DFTB and noncovalent interactions involving sulfur atoms. *J. Chem. Theory Comput.* **2013**, *9*, 3020–3025.
- (9) Goyal, P.; Ghosh, N.; Phatak, P.; Clemens, M.; Gaus, M.; Elstner, M.; Cui, Q. Proton storage site in bacteriorhodopsin: New insights from quantum mechanics/molecular mechanics simulations of microscopic pK(a) and infrared spectra. *J. Am. Chem. Soc.* **2011**, *133*, 14981–14997.

- (10) Riccardi, D.; Yang, S.; Cui, Q. Proton transfer function of carbonic anhydrase: Insights from QM/MM simulations. *Biochim. Biophys. Acta, Proteins Proteomics* **2010**, *1804*, 342–351.
- (11) Riccardi, D.; Konig, P.; Prat-Resina, X.; Yu, H. B.; Elstner, M.; Frauenheim, T.; Cui, Q. "Proton holes" in long-range proton transfer reactions in solution and enzymes: A theoretical analysis. *J. Am. Chem. Soc.* **2006**, *128*, 16302–16311.
- (12) Lear, J. D.; Wasserman, Z. R.; Degrado, W. F. Synthetic amphiphilic peptide models for protein ion channels. *Science* **1988**, *240*, 1177–1181.
- (13) Wu, Y. J.; Ilan, B.; Voth, G. A. Charge delocalization in proton channels, II: The synthetic LS2 channel and proton selectivity. *Biophys. J.* **2007**, *92*, 61–69.
- (14) Voth, G. A. The computer simulation of proton transport in biomolecular systems. *Front. Biosci.* **2003**, *8*, S1384–S1397.
- (15) Wu, Y. J.; Voth, G. A. A computer simulation study of the hydrated proton in a synthetic proton channel. *Biophys. J.* **2003**, *85*, 864–875.
- (16) Riccardi, D.; Schaefer, P.; Cui, Q. pK(a) calculations in solution and proteins with QM/MM free energy perturbation simulations: A quantitative test of QM/MM protocols. *J. Phys. Chem. B* **2005**, *109*, 17715–17733.
- (17) Yang, Y.; Yu, H. B.; York, D.; Cui, Q.; Elstner, M. Extension of the self-consistent-charge density-functional tight-binding method: Third-order expansion of the density functional theory total energy and introduction of a modified effective coulomb interaction. *J. Phys. Chem. A* **2007**, *111*, 10861–10873.
- (18) MacKerell, A. D.; Bashford, D.; Bellott, M.; Dunbrack, R. L.; Evanseck, J. D.; Field, M. J.; Fischer, S.; Gao, J.; Guo, H.; Ha, S.; Joseph-McCarthy, D.; Kuchnir, L.; Kuczera, K.; Lau, F. T. K.; Mattos, C.; Michnick, S.; Ngo, T.; Nguyen, D. T.; Prodhom, B.; Reiher, W. E.; Roux, B.; Schlenkrich, M.; Smith, J. C.; Stote, R.; Straub, J.; Watanabe, M.; Wiorkiewicz-Kuczera, J.; Yin, D.; Karplus, M. All-atom empirical potential for molecular modeling and dynamics studies of proteins. *J. Phys. Chem. B* **1998**, *102*, 3586–3616.
- (19) Mackerell, A. D.; Feig, M.; Brooks, C. L. Extending the treatment of backbone energetics in protein force fields: Limitations of gas-phase quantum mechanics in reproducing protein conformational distributions in molecular dynamics simulations. *J. Comput. Chem.* **2004**, *25*, 1400–1415.
- (20) Jorgensen, W. L.; Chandrasekhar, J.; Madura, J. D.; Impey, R. W.; Klein, M. L. Comparison of simple potential functions for simulating liquid water. *J. Chem. Phys.* **1983**, *79*, 926–935.
- (21) Hockney, R. W.; Eastwood, J. W. *Computer Simulation Using Particles*; Taylor & Francis: New York, 1988.
- (22) Wu, Y. J.; Chen, H. N.; Wang, F.; Paesani, F.; Voth, G. A. An improved multistate empirical valence bond model for aqueous proton solvation and transport. *J. Phys. Chem. B* **2008**, *112*, 467–482.
- (23) Plimpton, S. Fast parallel algorithms for short-range molecular dynamics. *J. Comput. Phys.* **1995**, *117*, 1–19.
- (24) Lippert, G.; Hutter, J.; Parrinello, M. A hybrid Gaussian and plane wave density functional scheme. *Mol. Phys.* **1997**, *92*, 477–487.
- (25) Becke, A. D. Density-functional exchange-energy approximation with correct asymptotic behavior. *Phys. Rev. A* **1988**, *38*, 3098–3100.
- (26) Lee, C. T.; Yang, W. T.; Parr, R. G. Development of the Colle–Salvetti correlation-energy formula into a functional of the electron density. *Phys. Rev. B* **1988**, *37*, 785–789.
- (27) Grimme, S.; Antony, J.; Ehrlich, S.; Krieg, H. A consistent and accurate ab initio parametrization of density functional dispersion correction (DFT-D) for the 94 elements H–Pu. *J. Chem. Phys.* **2010**, *132*, 154104.
- (28) Boese, A. D.; Doltsinis, N. L.; Handy, N. C.; Sprik, M. New generalized gradient approximation functionals. *J. Chem. Phys.* **2000**, *112*, 1670–1678.
- (29) Becke, A. D. Density-functional thermochemistry 0.3. The role of exact exchange. *J. Chem. Phys.* **1993**, *98*, 5648–5652.
- (30) Hartwigsen, C.; Goedecker, S.; Hutter, J. Relativistic separable dual-space Gaussian pseudopotentials from H to Rn. *Phys. Rev. B* **1998**, *58*, 3641–3662.
- (31) Laino, T.; Mohamed, F.; Laio, A.; Parrinello, M. An efficient linear-scaling electrostatic coupling for treating periodic boundary conditions in QM/MM simulations. *J. Chem. Theory. Comput.* **2006**, *2*, 1370–1378.
- (32) Laino, T.; Mohamed, F.; Laio, A.; Parrinello, M. An efficient real space multigrid OM/MM electrostatic coupling. *J. Chem. Theory. Comput.* **2005**, *1*, 1176–1184.
- (33) Blochl, P. E. Electrostatic decoupling of periodic images of plane-wave-expanded densities and derived atomic point charges. *J. Chem. Phys.* **1995**, *103*, 7422–7428.
- (34) VandeVondele, J.; Hutter, J. An efficient orbital transformation method for electronic structure calculations. *J. Chem. Phys.* **2003**, *118*, 4365–4369.
- (35) VandeVondele, J.; Krack, M.; Mohamed, F.; Parrinello, M.; Chassaing, T.; Hutter, J. QUICKSTEP: Fast and accurate density functional calculations using a mixed Gaussian and plane waves approach. *Comput. Phys. Commun.* **2005**, *167*, 103–128.
- (36) Brooks, B. R.; Brooks, C. L.; Mackerell, A. D.; Nilsson, L.; Petrella, R. J.; Roux, B.; Won, Y.; Archontis, G.; Bartels, C.; Boresch, S.; Caffisch, A.; Caves, L.; Cui, Q.; Dinner, A. R.; Feig, M.; Fischer, S.; Gao, J.; Hodoscek, M.; Im, W.; Kuczera, K.; Lazaridis, T.; Ma, J.; Ovchinnikov, V.; Paci, E.; Pastor, R. W.; Post, C. B.; Pu, J. Z.; Schaefer, M.; Tidor, B.; Venable, R. M.; Woodcock, H. L.; Wu, X.; Yang, W.; York, D. M.; Karplus, M. CHARMM: The biomolecular simulation program. *J. Comput. Chem.* **2009**, *30*, 1545–1614.
- (37) Konig, P. H.; Ghosh, N.; Hoffmann, M.; Elstner, M.; Tajkhorshid, E.; Frauenheim, T.; Cui, Q. Toward theoretical analysis of long-range proton transfer kinetics in biomolecular pumps. *J. Phys. Chem. A* **2006**, *110*, 548–563.
- (38) Cornell, W. D.; Cieplak, P.; Bayly, C. I.; Gould, I. R.; Merz, K. M.; Ferguson, D. M.; Spellmeyer, D. C.; Fox, T.; Caldwell, J. W.; Kollman, P. A. A 2nd generation force-field for the simulation of proteins, nucleic acids, and organic molecules. *J. Am. Chem. Soc.* **1995**, *117*, 5179–5197.
- (39) Randa, H. S.; Forrest, L. R.; Voth, G. A.; Sansom, M. S. P. Molecular dynamics of synthetic leucine-serine ion channels in a phospholipid membrane. *Biophys. J.* **1999**, *77*, 2400–2410.
- (40) Lin, I. C.; Seitsonen, A. P.; Coutinho-Neto, M. D.; Tavernelli, I.; Rothlisberger, U. Importance of van der Waals interactions in liquid water. *J. Phys. Chem. B* **2009**, *113*, 1127–1131.
- (41) Izvekov, S.; Voth, G. A. Ab initio molecular-dynamics simulation of aqueous proton solvation and transport revisited. *J. Chem. Phys.* **2005**, *123*, 044505.
- (42) Izvekov, S.; Swanson, J. M. J. Using force-matching to reveal essential differences between density functionals in ab initio molecular dynamics simulations. *J. Chem. Phys.* **2011**, *134*, 194109.
- (43) VandeVondele, J.; Mohamed, F.; Krack, M.; Hutter, J.; Sprik, M.; Parrinello, M. The influence of temperature and density functional models in ab initio molecular dynamics simulation of liquid water. *J. Chem. Phys.* **2005**, *122*, 14515.
- (44) Schmidt, J.; VandeVondele, J.; Kuo, I. F. W.; Sebastiani, D.; Siepmann, J. I.; Hutter, J.; Mundy, C. J. Isobaric–isothermal molecular dynamics simulations utilizing density functional theory: An assessment of the structure and density of water at near-ambient conditions. *J. Phys. Chem. B* **2009**, *113*, 11959–11964.
- (45) Rablen, P. R.; Lockman, J. W.; Jorgensen, W. L. Ab initio study of hydrogen-bonded complexes of small organic molecules with water. *J. Phys. Chem. A* **1998**, *102*, 3782–3797.
- (46) Shepherd, L. M. S.; Morrison, C. A. Simulating proton transport through a simplified model for trans-membrane proteins. *J. Phys. Chem. B* **2010**, *114*, 7047–7055.
- (47) Luzar, A.; Chandler, D. Hydrogen-bond kinetics in liquid water. *Nature* **1996**, *379*, 55–57.
- (48) Bandyopadhyay, S.; Chakraborty, S.; Bagchi, B. Secondary structure sensitivity of hydrogen bond lifetime dynamics in the protein hydration layer. *J. Am. Chem. Soc.* **2005**, *127*, 16660–16667.
- (49) Sinha, S. K.; Bandyopadhyay, S. Local heterogeneous dynamics of water around lysozyme: A computer simulation study. *Phys. Chem. Chem. Phys.* **2012**, *14*, 899–913.

(50) Markovitch, O.; Chen, H.; Izvekov, S.; Paesani, F.; Voth, G. A.; Agmon, N. Special pair dance and partner selection: Elementary steps in proton transport in liquid water. *J. Phys. Chem. B* **2008**, *112*, 9456–9466.

(51) Hou, G. H.; Zhu, X.; Elstner, M.; Cui, Q. A Modified QM/MM hamiltonian with the self-consistent-charge density-functional-tight-binding theory for highly charged QM regions. *J. Chem. Theory. Comput.* **2012**, *8*, 4293–4304.